

IRSRMamba: Infrared Image Super-Resolution via Mamba-based Wavelet Transform Feature Modulation Model

Yongsong Huang  *Student Member, IEEE, Tomo Miyazaki Member, IEEE, Xiaofeng Liu Member, IEEE, Shinichiro Omachi Senior Member, IEEE*

Abstract—Infrared (IR) image super-resolution faces challenges from homogeneous background pixel distributions and sparse target regions, requiring models that effectively handle long-range dependencies and capture detailed local-global information. Recent advancements in Mamba-based (Selective Structured State Space Model) models, employing state space models, have shown significant potential in visual tasks, suggesting their applicability for IR enhancement. In this work, we introduce IRSRMamba: Infrared Image Super-Resolution via Mamba-based Wavelet Transform Feature Modulation Model, a novel Mamba-based model designed specifically for IR image super-resolution. This model enhances the restoration of context-sparse target details through its advanced dependency modeling capabilities. Additionally, a new wavelet transform feature modulation block improves multi-scale receptive field representation, capturing both global and local information efficiently. Comprehensive evaluations confirm that IRSRMamba outperforms existing models on multiple benchmarks. This research advances IR super-resolution and demonstrates the potential of Mamba-based models in IR image processing. Code are available at <https://github.com/yongsongH/IRSRMamba>.

Index Terms—Super-resolution; Infrared image; State space models; Wavelet transformation; Image processing

I. INTRODUCTION

INFRARED imaging is always crucial for applications like security and interplanetary exploration[1], where visible light is limited[2–4]. The field has faced image quality challenges due to hardware constraints and environmental variability. To address this, researchers have turned to more cost-effective image processing algorithms, notably single image super-resolution (SISR)[5–7]. This method reconstructs high-resolution (HR) images from low-resolution (LR) counterparts using deep learning models that excel in learning non-linear mappings in complex spaces, ideal for SISR’s demands.

IR image super-resolution (IRSR) particularly struggles with balancing global and local information[8, 9] due to IR images’ uniform backgrounds and sparse details. Therefore, IRSR models need to adeptly handle long-range dependencies and integrate contextual information effectively for IR image patches[4, 5, 10, 11]. First, to address long-range dependency challenges in IR image restoration, we introduce a

pioneering Mamba-based model[12] as the backbone network, achieving state-of-the-art results in image segmentation and restoration[12–14]. The Mamba model uses the state space models to efficiently handle long-range dependencies, demonstrating effectiveness in extensive research[14–16]. For the sparse spatial data in IR images, leveraging the frequency domain can provide additional pattern details and improve global information recovery, as demonstrated in numerous studies[17–19]. Given that, we further propose a novel wavelet transform feature modulation block that enhances global and local information capture in multiscale feature representation. This block transforms feature maps into frequency-domain maps through wavelet transformation. When combined with large receptive field feature maps, they enable advanced contextual modeling by the Mamba backbone.

In summary, we introduce IRSRMamba: Infrared Image Super-Resolution via Mamba-based Wavelet Transform Feature Modulation Model, which marks a pioneering approach to IRSR: First, it employs a Mamba-based backbone network for the first time, effectively enhancing long-range dependency handling and improving the restoration of sparse IR image details. Second, we present a novel wavelet feature modulation block for multiscale shallow feature extraction, which utilizes wavelet transforms to adeptly capture multi-scale receptive field presentation. Finally, IRSRMamba establishes new benchmarks, outperforming existing methods on various datasets and leading in main performance metrics.

II. METHODOLOGY

A. Preliminaries

IR Image Super-Resolution: In the field of IRSR, current methodologies utilize paired training datasets denoted by $\{x_{ir}, y_{ir}\}$. Here, $x_{ir} \in \mathbb{R}^{\frac{H}{\mu} \times \frac{W}{\mu} \times C}$ represents the low-resolution IR images, and $y_{ir} \in \mathbb{R}^{H \times W \times C}$ represents the corresponding high-resolution IR images, with μ indicating the spatial upscaling factor that affects both the height (H) and width (W) dimensions. Here, C denotes the channel count of RGB images, typically three. **State Space Models:** Recent advancements in structured state-space sequence models (S4) are inspired by continuous linear time-invariant (LTI) systems. These map a 1-dimensional function or sequence $x(t) \in \mathbb{R}$ to $y(t) \in \mathbb{R}$ via an implicit latent state $h(t) \in \mathbb{R}^N$, described by the linear ordinary differential equations (ODE):

$$\begin{aligned} h(t) &= \mathbf{A}h(t-1) + \mathbf{B}x(t) \\ y(t) &= \mathbf{C}h(t) + \mathbf{D}x(t) \end{aligned} \quad (1)$$

This work was supported by JSPS KAKENHI Grant Number JP23KJ0118. (Corresponding author: Yongsong Huang )

Yongsong Huang is with Tohoku University (and Yale University), Sendai 9808579, Japan. (e-mail: hys@dc.tohoku.ac.jp)

Prof. Tomo Miyazaki and Prof. Shinichiro Omachi with Lab for Image Information Communications, Tohoku University, Sendai 9808579, Japan.

Prof. Xiaofeng Liu is with Yale University, New Haven 06519, USA.

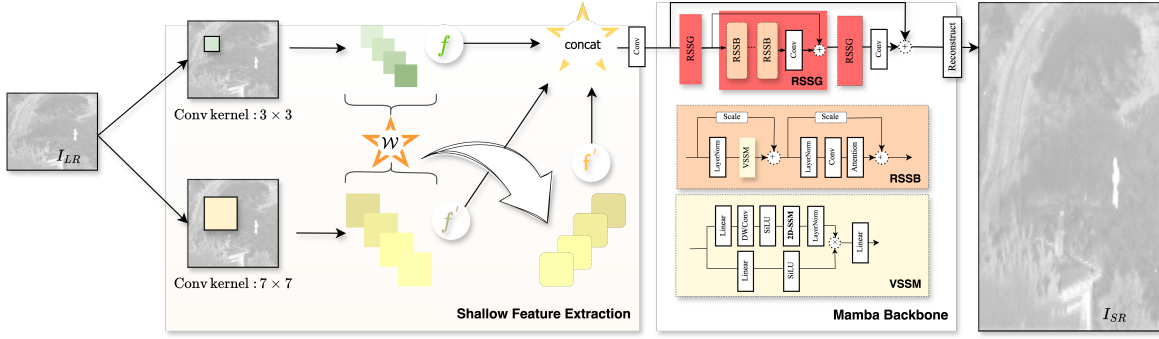


Fig. 1. The architecture of IRSRMamba with the input image data $I_{LR} \in x_{ir}$ and $concat$ denotes the concat operation. IRSRMamba model includes shallow feature extraction, Mamba backbone network and reconstruction tail. For shallow feature extraction: there are three different feature maps shown here: the small receptive field feature map f from the 3×3 convolutional kernel, the large receptive field 7×7 feature map f' and the wavelet transform modulated feature map defined as f'' . The Wavelet Transform Feature Modulation Block \mathcal{W} shown in Fig.2. And the Mamba backbone network is based on Residual State-Space Groups (RSSG), which include the Residual State-Space Block (RSSB), the Vision State-Space Module (VSSM), and the 2D Selective Scan Module (2D-SSM, see Fig.3). Best viewed in color.

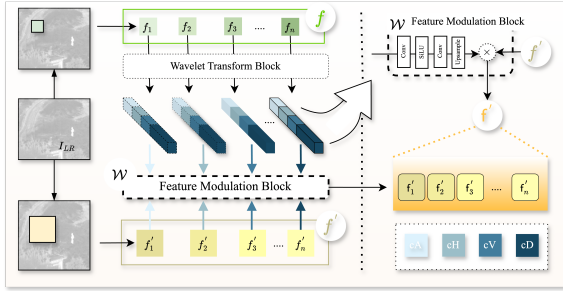


Fig. 2. The architecture of Wavelet Transform Feature Modulation Block. n denotes the feature maps of different channels, and feature modulation happens between the corresponding feature maps.

where $\mathbf{A} \in \mathbb{R}^{N \times N}$, $\mathbf{B} \in \mathbb{R}^{N \times 1}$, $\mathbf{C} \in \mathbb{R}^{1 \times N}$, and $\mathbf{D} \in \mathbb{R}$. To apply these in deep learning, these continuous parameters are discretized using the zero-order hold (ZOH) method with a timescale parameter Δ , resulting in:

$$\begin{aligned} \bar{\mathbf{A}} &= \exp(\Delta \mathbf{A}) \\ \bar{\mathbf{B}} &= (\Delta \mathbf{A})^{-1} (\exp(\Delta \mathbf{A}) - \mathbf{I}) \cdot \Delta \mathbf{B} \end{aligned} \quad (2)$$

The discretized equations, suitable for RNN implementation, are:

$$\begin{aligned} h_t &= \bar{\mathbf{A}} h_{t-1} + \bar{\mathbf{B}} x_t \\ y_t &= \mathbf{C} h_t + \mathbf{D} x_t \end{aligned} \quad (3)$$

These equations can also be transformed into a CNN framework where the convolution operation is represented as:

$$\begin{aligned} \bar{\mathbf{K}} &\triangleq (\mathbf{C}\bar{\mathbf{B}}, \mathbf{C}\bar{\mathbf{A}}\bar{\mathbf{B}}, \dots, \mathbf{C}\bar{\mathbf{A}}^{L-1}\bar{\mathbf{B}}), \\ \mathbf{y} &= \mathbf{x} \circledast \bar{\mathbf{K}} \end{aligned} \quad (4)$$

where L is the length of the input sequence and $\bar{\mathbf{K}} \in \mathbb{R}^L$ serves as a structured convolution kernel. \circledast denotes convolution operation.

B. IRSRMamba Architecture

IRSRMamba introduces Mamba-based to the IRSR domain for the first time, aiming to help the model establish the contextual dependencies of IR image patches to better restore

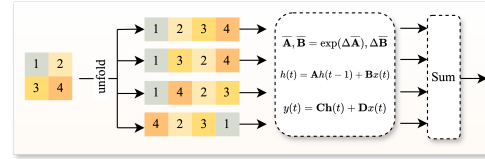


Fig. 3. The architecture of 2D-Selective Scan Module (2D-SSM).

detailed textures. As illustrated in Figure.1, the IRSRMamba consists of three modules: shallow feature extraction, Mamba backbone, and reconstruction tail. Initially, the model processes a low-quality input image $I_{LR} \in \mathbb{R}^{H \times W \times 3}$ through a 3×3 convolution to derive initial shallow features. These features are then expanded using both a 7×7 convolutional kernel for broader context and a wavelet transform feature modulation block \mathcal{W} (see Fig.2), enhancing the feature maps with rich, scale-specific details.

Subsequent deep feature extraction involves multiple RSSG, each containing several RSSB to progressively refine these features. RSSB in backbone networks to replace the traditional Transformer flow of Norm \rightarrow Attention \rightarrow Norm \rightarrow MLP. Unlike simple swaps of Attention with SSM, which yielded suboptimal results, RSSB integrates a VSSM and a LayerNorm (LN) to effectively capture spatial long-term dependencies. Additionally, RSSB incorporates a learnable scale factor $s \in \mathbb{R}^C$, which enhances the adaptability of skip connections by dynamically scaling the original features. The transformation within the RSSB is formulated as:

$$Z^i = \text{VSSM}(\text{LN}(F_D^i)) + s \cdot F_D^i, \quad (5)$$

where F_D^i denotes the input deep features at the i -th layer. $s \cdot F_D^i$ represents the scaled skip connection. Z^i is the output of the RSSB

Further, VSSM is designed to capture long-range dependencies utilizing a state-space equation, as depicted in Figure.1. According to [20], the input feature $X \in \mathbb{R}^{H \times W \times C}$ undergoes processing through two parallel pathways. In the first pathway, feature channels are expanded to λC using a linear layer, processed through a depth-wise convolution and a SiLU activation σ , followed by a 2D-SSM layer and LayerNorm.

Concurrently, in the second pathway, channels are similarly expanded and activated via σ . Outputs from these pathways are combined using the Hadamard product and then projected back to C channels to produce the output X_{out} maintaining the original dimensions:

$$\begin{aligned} X_1 &= \text{LN}(2\text{D-SSM}(\sigma(\text{DWConv}(\text{Linear}(X)))))) \\ X_2 &= \sigma(\text{Linear}(X)) \\ X_{\text{out}} &= \text{Linear}(X_1 \otimes X_2) \end{aligned} \quad (6)$$

DWConv denotes depth-wise convolution, and \otimes represents the Hadamard product. This structure ensures efficient integration and transformation of feature channels, enhancing the module’s ability to manage spatial relationships within the data. The standard Mamba framework[12], originally designed for processing sequential data, encounters limitations with non-causal data such as images. In our work, 2D-SSM as per[20], converts 2D image features into 1D sequences across four scanning directions. These sequences are analyzed using discrete state-space equations to capture long-range dependencies (see Fig.3). The sequences are then summed and reshaped to restore the original 2D format, effectively preserving spatial information and enhancing image processing capabilities.

C. Wavelet Transform Feature Modulation Block

In IRSRMamba, the Wavelet Transform Feature Modulation Block \mathcal{W} is crucial for enhancing shallow features. It applies wavelet transforms to small receptive field feature maps, boosting the large receptive field maps within the frequency domain. This approach introduces a novel method for extracting both local and global information from the multi-scale features of IR images. This block initiates with an input x_{ir} . The modulation process begins with the application of two distinct convolutional modules, $\text{Conv}_{3 \times 3}$ and $\text{Conv}_{7 \times 7}$, which extract features at different scales:

$$\begin{aligned} f &= \text{Conv}_{3 \times 3}(x_{ir}) \\ f' &= \text{Conv}_{7 \times 7}(x_{ir}) \end{aligned} \quad (7)$$

Here, f captures finer details using a 3×3 convolution kernel, while f' secures broader contextual information via a 7×7 kernel. Subsequently, the small-scale feature map f is processed through the wavelet transform block (WTB), $cA, cH, cV, cD = \text{WTB}(f)$ resulting in four components that detail various directional textures:

$$f_{\text{wavelet}} = \text{Concat}(cA, cH, cV, cD) \quad (8)$$

These components cA (approximation), cH (horizontal detail), cV (vertical detail), and cD (diagonal detail) each emphasize unique spatial frequencies of the image. This enhanced map f' is utilized to modulate the f through the \mathcal{W} :

$$f' = f' \otimes \mathcal{F}_{\uparrow}(\text{Conv}_{3 \times 3}(\sigma(\text{Conv}_{3 \times 3}(f_{\text{wavelet}})))) \quad (9)$$

\mathcal{F}_{\uparrow} represents the up-sampling layer. The final step involves combining the modulated f' with the f and f' to form an integrated feature map f_{combined} :

$$f_{\text{combined}} = \text{Concat}(f, f', f') \quad (10)$$

TABLE I
ABLATION EXPERIMENT WITH THE PERFORMANCE OF DIFFERENT BACKBONE NETWORKS ACROSS DIFFERENT TEST DATASETS.

Scale $\times 2$	MambaIR (Pure)	\rightarrow w/Multiscale	\rightarrow w/Wavelet Modulation
result-A	38.66/0.9372	39.16/0.9427	39.33/0.9439 [0.67dB \uparrow]
result-C	39.49/0.9487	40.00/0.9536	40.21/0.9548 [0.72dB \uparrow]
CVC10	43.98/0.9704	44.16/0.9714	44.50/0.9719 [0.52dB \uparrow]

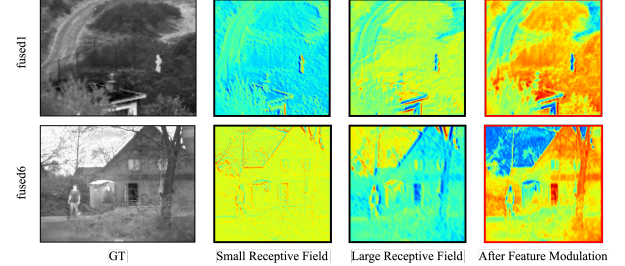


Fig. 4. Feature map visualization comparison. From left to right: GT from result-A dataset, feature maps applied with the 3×3 convolutional kernel, feature maps from the 7×7 convolutional kernel, feature maps after wavelet transform feature modulation.

III. EXPERIMENT RESULTS & DETAILS

A. Datasets and Metrics

In this study, we selected 265 high-quality IR images from the well-known M3FD dataset[21] as HR samples. The corresponding LR images were generated via bicubic downsampling. To facilitate a fair comparison with existing methods, we assessed quantitative metrics and reconstruction quality using IRSRMamba and other models on benchmark datasets result-A[5, 22] and result-C[5, 23]. Additionally, the CVC10 dataset[24] was employed to evaluate the generalization ability of our methods across diverse datasets. Image reconstruction quality was assessed using the Peak Signal-to-Noise Ratio (PSNR), Mean Squared Error (MSE), and the Structural Similarity Index (SSIM). We set the learning rate to $1e^{-4}$ and the batch size to 32. For optimization, Adam was used. Implementation was carried out using the PyTorch framework on NVIDIA A6000 GPUs. The performance of IRSRMamba was assessed exclusively on the (Y) channel of images.

B. Ablation Experiments

To evaluate the efficacy of IRSRMamba, we conducted a series of ablation studies across various test datasets, as summarized in Table.I. The baseline configuration, MambaIR (Pure), was incrementally enhanced with multiscale features and wavelet modulation. These modifications led to consistent improvements in both PSNR and SSIM across all datasets.

For the result-A dataset, the integration of multiscale features enhanced the PSNR from 38.66 to 39.16 and the SSIM from 0.9372 to 0.9427. The incorporation of wavelet modulation further elevated these metrics to 39.33 and 0.9439, respectively, resulting in a cumulative gain of 0.67 dB. Similarly, the result-C dataset observed a PSNR increase from 39.49 to 40.21 and SSIM from 0.9487 to 0.9548, marking a peak improvement of 0.72 dB with the full enhancements. Further details are shown in Table.I.

TABLE II

THE AVERAGE RESULTS OF (PSNR \uparrow MSE \downarrow SSIM \uparrow) WITH SCALE FACTOR OF 4 & 2 ON DATASETS RESULT-A & RESULT-C & CVC10. BEST AND SECOND-BEST PERFORMANCES ARE MARKED IN **BOLD** AND UNDERLINED, RESPECTIVELY.

Scale	Methods	result-A			result-C			CVC10		
		PSNR \uparrow	MSE \downarrow	SSIM \uparrow	PSNR \uparrow	MSE \downarrow	SSIM \uparrow	PSNR \uparrow	MSE \downarrow	SSIM \uparrow
$\times 2$	EDSR[<i>CVPRW 2017</i>] [25]	39.0493	11.8196	0.9414	39.8902	8.9865	0.9528	44.1770	2.7845	0.9713
	ESRGAN[<i>ECCVW 2018</i>] [26]	38.7738	12.5212	0.9384	39.6111	9.5793	0.9500	44.0974	2.8477	0.9709
	FSRCNN[<i>ECCV 2016</i>] [27]	39.1175	11.3761	0.9426	39.9858	8.6899	0.9535	44.1253	2.8162	0.9710
	SRGAN[<i>CVPR 2017</i>] [28]	39.0401	11.9024	0.9414	39.8678	9.0586	0.9527	44.1736	2.7851	0.9713
	SwinIR[<i>ICCV 2021</i>] [29]	38.6899	12.5694	0.9374	39.5215	9.6530	0.9492	43.9980	2.8926	0.9704
	SRCNN[<i>T-PAMI 2015</i>] [30]	38.9671	11.7216	0.9414	39.8642	8.8857	0.9524	44.0038	2.9084	0.9707
	RCAN[<i>ECCV 2018</i>] [31]	38.8145	12.4926	0.9391	39.7075	9.4220	0.9511	44.1205	2.8170	0.9713
	PSRGAN[<i>SPL 2021</i>] [5]	<u>39.2146</u>	<u>11.2409</u>	<u>0.9429</u>	<u>40.0543</u>	<u>8.6101</u>	0.9539	<u>44.2377</u>	<u>2.7454</u>	0.9713
	ShuffleMixer(tiny)[<i>NIPS'22</i>] [32]	39.0465	11.7605	0.9414	39.8766	8.9680	0.9527	44.1408	2.8113	0.9713
	ShuffleMixer (base)[<i>NIPS'22</i>] [32]	38.8066	12.3718	0.9388	39.6347	9.4864	0.9503	44.0357	2.8809	0.9710
	HAT[<i>CVPR 2023 SOTA</i>] [33]	38.7754	12.4528	0.9384	39.6346	9.5132	0.9500	44.1080	2.8244	0.9709
	RGT[<i>ICLR 2024 SOTA</i>] [34]	39.1642	11.3382	0.9429	40.0522	8.6033	<u>0.9540</u>	44.2311	2.7358	<u>0.9717</u>
IRSRMamba (Ours)	39.3341	10.9182	0.9439	40.2150	8.3396	0.9548	44.5098	2.5673	0.9719	
$\times 4$	EDSR[<i>CVPRW 2017</i>] [25]	34.5219	30.1273	0.8548	35.1740	23.9917	0.8723	40.1190	6.8819	0.9482
	ESRGAN[<i>ECCVW 2018</i>] [26]	33.6895	34.7337	0.8500	34.1650	28.9017	0.8679	37.9780	10.9641	0.9455
	FSRCNN[<i>ECCV 2016</i>] [27]	33.8556	34.4909	0.8446	34.5272	27.4495	0.8636	38.7856	9.5482	0.9421
	SRGAN[<i>CVPR 2017</i>] [28]	<u>34.5807</u>	<u>29.6927</u>	<u>0.8556</u>	<u>35.2076</u>	<u>23.7701</u>	<u>0.8728</u>	<u>40.1479</u>	<u>6.8162</u>	0.9483
	SwinIR[<i>ICCV 2021</i>] [29]	34.4321	30.6081	0.8537	35.0329	24.6490	0.8710	39.9062	7.1886	0.9479
	SRCNN[<i>T-PAMI 2015</i>] [30]	33.6839	34.9181	0.8415	34.2348	28.6115	0.8568	38.0976	10.7588	0.9279
	RCAN[<i>ECCV 2018</i>] [31]	34.4280	30.8815	0.8528	35.0823	24.6507	0.8705	40.0805	6.9225	<u>0.9484</u>
	PSRGAN[<i>SPL 2021</i>] [5]	34.4595	30.3760	0.8540	35.1023	24.3147	0.8715	39.9533	7.1274	0.9471
	ShuffleMixer(tiny)[<i>NIPS'22</i>] [32]	34.5440	29.9449	0.8550	35.1640	23.9705	0.8723	40.0756	6.9296	0.9478
	ShuffleMixer (base)[<i>NIPS'22</i>] [32]	34.4507	30.6955	0.8538	35.0911	24.3745	0.8714	40.0120	7.0622	0.9477
	HAT[<i>CVPR 2023 SOTA</i>] [33]	34.4947	30.4086	0.8542	35.1239	24.3103	0.8713	40.0934	6.9078	0.9478
	RGT[<i>ICLR 2024 SOTA</i>] [34]	34.4262	30.7665	0.8534	35.0752	24.5105	0.8710	39.9794	7.0851	0.9476
IRSRMamba (Ours)	34.6501	29.2504	0.8569	35.2825	23.3929	0.8738	40.3810	6.5029	0.9492	

The visualized experiments (see Fig.4) illustrate the efficacy of our proposed enhancements. Using wavelet transform feature modulation significantly enriches feature map detail and contrast, crucial for superior image reconstruction.

C. Qualitative Result

In our quantitative analysis, we compared the performance of IRSRMamba against a range of state-of-the-art super-resolution methods across different datasets and scaling factors, as detailed in Table.II. These methods include EDSR[25], ESRGAN[26], FSRCNN [27], SRGAN [28], SwinIR[29], SRCNN[30], RCAN[31], PSRGAN[5], ShuffleMixer[32], HAT[33], and RGT[34], which have been benchmarks in recent years for SR tasks.

Our method consistently outperformed all compared models across three main performance metrics: PSNR, MSE, and SSIM. For instance, in the $\times 2$ scale factor on the result-A dataset, IRSRMamba achieved the highest PSNR at 39.3341, the lowest MSE at 10.9182, and the top SSIM at 0.9439, significantly surpassing the closest competitor, RGT[34], which scored slightly lower across these metrics.

On the other hand, Figure.5 showcases the superior super-resolution capabilities of IRSRMamba, as evidenced in results-A and results-C with scaling factors of $\times 2$ and $\times 4$, respectively. Our method excels in detail preservation and edge sharpness, delivering more precise reconstructions of fine details like text and architectural features compared to established methods, affirm IRSRMamba's advanced performance and potential for real-world imaging applications.

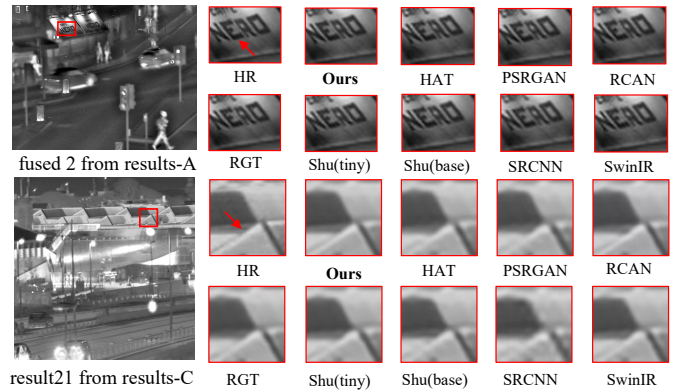


Fig. 5. **Top** The SR results of fused2 from results-A with scale factor of $\times 2$. **Below** The SR results of result21 from results-C with scale factor of $\times 4$.

IV. CONCLUSION

In this study, we introduce IRSRMamba, a novel IR image super-resolution model utilizing a Mamba-based backbone for enhanced long-range dependency handling and detail restoration in sparse IR images. The model also incorporates a wavelet feature modulation module for effective multiscale shallow feature extraction. Demonstrating superior performance on various datasets, IRSRMamba establishes new benchmarks in the field, excelling in key metrics such as PSNR, MSE, and SSIM. Our approach holds promise for providing constructive insights into the exploration of Mamba models in the field of IR image enhancement, potentially guiding future developments in this area.

REFERENCES

- [1] P. M. Harvey *et al.*, “First science results from sofia/forcast: Super-resolution imaging of the s140 cluster at 37 μm ,” *The Astrophysical Journal Letters*, vol. 749, no. 2, p. L20, 2012.
- [2] S. Liang *et al.*, “Dasr: Dual-attention transformer for infrared image super-resolution,” *Infrared Physics & Technology*, vol. 133, p. 104837, 2023.
- [3] X. Chen *et al.*, “Modeling thermal infrared image degradation and real-world super-resolution under background thermal noise and streak interference,” *IEEE Transactions on Circuits and Systems for Video Technology*, 2024.
- [4] T. Ma *et al.*, “Msma-net: An infrared small target detection network by multi-scale super-resolution enhancement and multi-level attention fusion,” *IEEE Transactions on Geoscience and Remote Sensing*, 2023.
- [5] Y. Huang, Z. Jiang, R. Lan, S. Zhang, and K. Pi, “Infrared image super-resolution via transfer learning and psrgan,” *IEEE Signal Processing Letters*, vol. 28, pp. 982–986, 2021.
- [6] Z. Jiang *et al.*, “Difference value network for image super-resolution,” *IEEE Signal Processing Letters*, vol. 28, pp. 1070–1074, 2021.
- [7] D. Zhang *et al.*, “Joint motion deblurring and super-resolution for single image using diffusion model and gan,” *IEEE Signal Processing Letters*, 2024.
- [8] Y. Chen *et al.*, “Efficient multi-scale cosine attention transformer for image super-resolution,” *IEEE Signal Processing Letters*, 2023.
- [9] B. Zhou *et al.*, “Structure and texture preserving network for real-world image super-resolution,” *IEEE Signal Processing Letters*, vol. 29, pp. 2173–2177, 2022.
- [10] H. Yongsong *et al.*, “Infrared image super-resolution: Systematic review, and future trends,” *arXiv preprint arXiv:2212.12322*, 2023.
- [11] Z. Zhao *et al.*, “Modality conversion meets super-resolution: A collaborative framework for high-resolution thermal uav image generation,” *IEEE Transactions on Geoscience and Remote Sensing*, 2024.
- [12] A. Gu and T. Dao, “Mamba: Linear-time sequence modeling with selective state spaces,” *arXiv preprint arXiv:2312.00752*, 2023.
- [13] H. Guo *et al.*, “Mambair: A simple baseline for image restoration with state-space model,” *arXiv preprint arXiv:2402.15648*, 2024.
- [14] L. Zhu *et al.*, “Vision mamba: Efficient visual representation learning with bidirectional state space model,” *arXiv preprint arXiv:2401.09417*, 2024.
- [15] H. Zhang *et al.*, “A survey on visual mamba,” *arXiv preprint arXiv:2404.15956*, 2024.
- [16] X. Wang *et al.*, “State space model for new-generation network alternative to transformers: A survey,” *arXiv preprint arXiv:2404.09516*, 2024.
- [17] M. Xue *et al.*, “Low-light image enhancement via clip-fourier guided wavelet diffusion,” *ACM MM*, 2024.
- [18] H. Jiang *et al.*, “Low-light image enhancement with wavelet-based diffusion models,” *ACM Transactions on Graphics (TOG)*, vol. 42, no. 6, pp. 1–14, 2023.
- [19] B. Liu *et al.*, “Mwln: Multilevel wavelet learning network for continuous-scale remote sensing image super-resolution,” *IEEE Geoscience and Remote Sensing Letters*, 2023.
- [20] Y. Liu *et al.*, “Vmamba: Visual state space model,” *arXiv preprint arXiv:2401.10166*, 2024.
- [21] J. Liu *et al.*, “Target-aware dual adversarial learning and a multi-scenario multi-modality benchmark to fuse infrared and visible for object detection,” in *Proceedings of the IEEE/CVF CVPR*, pp. 5802–5811, 2022.
- [22] Y. o. Liu, “Infrared and visible image fusion with convolutional neural networks,” *INT J WAVELETS MULTI*, vol. 16, no. 03, p. 1850018, 2018.
- [23] Y. Zhang *et al.*, “Infrared and visual image fusion through infrared feature extraction and visual information preservation,” *INFRARED PHYS TECHN*, vol. 83, pp. 227–237, 2017.
- [24] F. B. Campo *et al.*, “Multimodal stereo vision system: 3d data extraction and algorithm evaluation,” *IEEE Journal of Selected Topics in Signal Processing*, vol. 6, no. 5, pp. 437–446, 2012.
- [25] B. Lim *et al.*, “Enhanced deep residual networks for single image super-resolution,” in *Proceedings of the IEEE CVPRW*, pp. 136–144, 2017.
- [26] X. Wang, K. Yu, S. Wu, J. Gu, Y. Liu, C. Dong, Y. Qiao, and C. Change Loy, “Esrgan: Enhanced super-resolution generative adversarial networks,” in *Proceedings of the European conference on computer vision (ECCV) workshops*, pp. 0–0, 2018.
- [27] C. Dong *et al.*, “Accelerating the super-resolution convolutional neural network,” in *ECCV*, pp. 391–407, Springer, 2016.
- [28] C. Ledig *et al.*, “Photo-realistic single image super-resolution using a generative adversarial network,” in *Proceedings of the IEEE/CVF CVPR*, pp. 4681–4690, 2017.
- [29] J. Liang *et al.*, “Swinir: Image restoration using swin transformer,” in *Proceedings of the IEEE/CVF ICCV*, pp. 1833–1844, 2021.
- [30] C. Dong *et al.*, “Image super-resolution using deep convolutional networks,” *IEEE transactions on pattern analysis and machine intelligence*, vol. 38, no. 2, pp. 295–307, 2015.
- [31] Y. Zhang *et al.*, “Image super-resolution using very deep residual channel attention networks,” in *Proceedings of the ECCV*, pp. 286–301, 2018.
- [32] L. Sun *et al.*, “Shufflemixer: An efficient convnet for image super-resolution,” *Advances in Neural Information Processing Systems*, vol. 35, pp. 17314–17326, 2022.
- [33] X. Chen *et al.*, “Activating more pixels in image super-resolution transformer,” in *Proceedings of the IEEE/CVF CVPR*, pp. 22367–22377, June 2023.
- [34] Z. Chen, Y. Zhang, J. Gu, L. Kong, and X. Yang, “Recursive generalization transformer for image super-resolution,” in *ICLR*, 2024.